

State transfer in dissipative and dephasing environments

M.L. Hu^a

School of Science, Xi'an University of Posts and Telecommunications, Xi'an 710061, China

Received: date / Revised version: date

Abstract. By diagonalization of a generalized superoperator for solving the master equation, we investigated effects of dissipative and dephasing environments on quantum state transfer, as well as entanglement distribution and creation in spin networks. Our results revealed that under the condition of the same decoherence rate γ , the detrimental effects of the dissipative environment are more severe than that of the dephasing environment. Beside this, the critical time t_c at which the transfer fidelity and the concurrence attain their maxima arrives at the asymptotic value $t_0 = \pi/2\lambda$ quickly as the spin chain length N increases. The transfer fidelity of an excitation at time t_0 is independent of N when the system subjects to dissipative environment, while it decreases as N increases when the system subjects to dephasing environment. The average fidelity displays three different patterns corresponding to $N = 4r + 1$, $N = 4r - 1$ and $N = 2r$. For each pattern, the average fidelity at time t_0 is independent of r when the system subjects to dissipative environment, and decreases as r increases when the system subjects to dephasing environment. The maximum concurrence also decreases as N increases, and when $N \rightarrow \infty$, it arrives at an asymptotic value determined by the decoherence rate γ and the structure of the spin network.

PACS. 03.67.-a Quantum information – 03.67.Mn Entanglement production, characterization, and manipulation – 03.65.Yz Decoherence; open systems; quantum statistical methods

1 Introduction

An important and new emerging pursuit of quantum information processing (QIP) task is the high-fidelity transmission of quantum states across a pre-engineered quantum spin network. This is so because when performing any QIP tasks, one needs to exchange quantum information between distant nodes (e.g., the core processor, storage, etc.) of a quantum computer. In general, the basic idea of transmitting a quantum state from one location of a network to another proceeds in three steps [1]. The first step is the initialization of the spin medium in a fiducial pure state, then the sender Alice encodes the state needs to be transmitted at one node of the network, and time evolution of the system for a proper interval of time, finally, the state will be recovered at the nodes belonging to the receiver Bob with certain fidelity. Particularly, the quantum channel may enable state transfer with fidelity better than any classical communication channel.¹

Since the seminal work of Bose [1], in which the author demonstrated that an unmodulated ferromagnetic spin chain with Heisenberg interactions can be used as a channel for short distance quantum communication, there has been an increasing discussion of quantum state transfer in various physical systems in the literature. Among such systems, the solid-state quantum system with spin-spin in-

teractions offers an excellent theoretical framework for designing networks for perfect state transfer (PST) [1, 2, 3, 4, 5, 6, 7, 8, 9, 10, 11, 12, 13, 14, 15, 16]. Particularly, Christandl et al. suggested a PST algorithm which can transfer an arbitrary quantum state between the opposite ends of a spin chain or the two antipodes of the one-link and the two-link hypercubes [3, 4]. Zhang and Long et al. [13] realized this PST algorithm in a three-qubit XX spin chain using liquid nuclear magnetic resonance (NMR) system. Since then, quantum spin networks as an ideal communication channel to realize QIP tasks have been extensively studied. Shi et al. [6] presented a series of perfect spin channels according to the spectrum-parity-matching condition they derived. Then, Kostak et al. [14] established a general formalism for engineering spin Hamiltonians for PST in spin networks of arbitrary topology and coupling configuration. Christandl's innovative works [3, 4] were extended by Jafarizadeh and Sufiani in a recent work [15], in which they adopted distance-regular graphs as spin networks and found that any such network can achieve unit fidelity of state transfer over arbitrarily long distances. Moreover, D'Amico et al. [10] showed that one can create and distribute entanglement with an interaction-modulated Y-shaped spin network, particularly, with a slightly complicated bifurcation structure, one can even freeze the entanglement by applying a phase flip to one spin out of each pair.

Apart from the aforementioned protocols which mainly concentrated on quantum spin chains with only nearest-

^a e-mail: mingliang0301@xupt.edu.cn

¹ The context of a footnote.

neighbor (NN) couplings, in Ref. [17] Paternostro et al. presented another scheme which enables nearly optimal state transfer in imperfect artificial spin networks with all the qubits are mutually coupled. Then Kay demonstrated that PST is also possible in the presence of next-nearest-neighbor (NNN) couplings [18]. Moreover, compared to the case where the system contains only two-spin interactions, the authors in Ref. [19] showed that the speed of quantum state transfer across the XY spin chain can be significantly increased by introducing the three-spin interaction. Besides the spin-1/2 systems, state transfer efficiency of a bilinear-biquadratic (BB) spin-1 Heisenberg chain has also been discussed [20].

Most recently, Franco et al. [21] presented a control-limited scheme [22] for PST through a pre-engineered spin chain. Different from the previous schemes whose achievements relies crucially on the initialization of the channel state, Franco et al. [21] demonstrated that such state initialization is in fact inessential to the performance of the protocol if proper encoding at the end of the chain is performed. The key requirements for their scheme are the arrangement of proper time evolution and the performance of clean projective measurements on the two end spins, which considerably relaxes the prerequisites for obtaining reliable state transfer across interacting-spin systems. Motivated by this innovative work, Markiewicz and Wieśniak [23] proposed a special type of encoding strategy for PST of a two-qubit state, where no remote-cooperated global state initialization and any additional communication are needed.

Besides these exciting progresses in this direction, however, one cannot neglect the fact that real quantum system is very susceptible to decoherence [24, 25, 26, 27, 28, 29, 30, 31, 32, 33, 34, 35]. For nearly all QIP tasks, the quantum system of interest will inevitably be interacted with its surrounding environments (or the thermal reservoirs). This unavoidable mutual interaction often cause the initial state of the system becomes entangled with the environments in an uncontrollable way, and it is this entanglement of the system with the environment that induces decoherence. The decoherence can affects quantum interferences of quantum systems and leads to the degradation of quantum coherence, and thus becomes a serious limiting factor baffling the physical realization of a quantum computer. Since the system of interest is inevitably subject to decoherence and decay processes, no matter how much they may be screened from the external environments, it would seem important to consider possible methods to minimize, delay, or even eliminate this unwanted detrimental effects of environments in the practical realization of various QIP tasks [36, 37].

Dissipation and dephasing are two important sources of decoherence in practice, and their effects on entanglement dynamics have been analyzed very recently in Refs. [26, 27, 28, 29] for the special case of two spin-halves where an analytical treatment is possible. The results revealed that the entanglement dynamics depends not only on the parameters of the system, but also on the system-environment coupling strength and the initial states of

concern. How these decoherence modes affect quantum state transfer fidelity in a spin chain is an interesting and urgent problem needs to be solved, and it is also of both theoretical and experimental significance. We will address this question in the present paper. The contents are organized as follows. In Section 2, we introduced the technique for solving the Lindblad form of the master equation. Based on this technique, we obtained the time evolution operator of the system and the explicit form of the state transfer fidelity. Then in Section 3, we investigated dynamics of the state transfer fidelity with the system subjects to dissipative and dephasing environments, where we concentrated on several ideal spin channels in the absence of decoherence, and aimed at revealing the extent to which the decoherence affects quantum state transfer. Section 4 is devoted to the analysis of the effects of the dissipative and dephasing environments on entanglement distribution and creation between distant parties through a pre-engineered spin network. Finally, we concluded this paper with a short discussion in Section 5.

2 Solution of the master equation

As pointed in Section 1, the unavoidable mutual interaction of an open quantum system with its surrounding environment is an important source of decoherence. In order to describe such phenomena, a master equation approach can be used. In the present work, we investigate how the dissipative and the dephasing environments affect quantum state transfer, as well as entanglement distribution and creation through a pre-engineered spin network. We assume that during the decoherence processes each spin of the system interacts only, and independently, with its own environment (this assumption is legitimate provided the constituents composing the quantum system are separated by distances large enough, however, it may not be totally valid in the case where the spins are close enough to each other to couple strongly enough), then in the Markovian limit, the dynamics of the system can be described by a general quantum master equation (ME) of the Lindblad form [38, 39]

$$\frac{d\rho}{dt} = -i[\hat{H}, \rho] + \sum_n \mathcal{L}_n \rho, \quad (1)$$

where \hat{H} and ρ denote, respectively, the Hamiltonian and the density operator of the system, and the summation on the second term of the right-hand side of this equation runs over all the spins involved. \mathcal{L}_n refers to the Lindblad superoperator, which describes the independent interaction between each spin and the environment and can be written, under weak system-environment interaction and in the Markovian limit, as [38]

$$\mathcal{L}_n \rho = \frac{\gamma}{2}(2c_n \rho c_n^\dagger - c_n^\dagger c_n \rho - \rho c_n^\dagger c_n). \quad (2)$$

Here γ is the phenomenological parameter that describes the coupling strength of a qubit with its local environment.

The system-environment coupling operator is given by $c_n = \sigma_n^-$ for the dissipative environment, and $c_n = \sigma_n^+ \sigma_n^-$ for the dephasing environment. The first term on the right-hand side of Eq. (1) generates a coherent unitary evolution of the system, while the second term represents the decoherence effects of the environment on the system and generates an incoherent dynamics of the system.

In order to assess the extent to which the decoherence affects dynamics of a correlated spin system, one must first try to obtain solutions of the ME. Although for systems with certain symmetries, the ME can be solved by adopting the superoperator method [40] or the Lie algebraic method (see, e.g., Ref. [41] and references therein). For general cases, however, this is still an uneasy task because the ME expressed in Eq. (1) contains terms coupled with each other in a non-trivial way. Although one can convert it to an equivalent c -number partial differential equation [42] and then solve it numerically using the conventional Runge-kutta algorithm; however, for system with large number of spins, this is still a troublesome task for it wasting too much computation resources to obtain the density operator $\rho(t)$, and the situation becomes even more cumbersome when one performs simulations of $\rho(t)$ with different initial states because for every initial state one must perform the Runge-kutta algorithm again to obtain the solutions of the ME. In order to circumvent this quandary, in the present paper we resort to another technique to solve the ME, as one will see, the success of this technique depends solely on the exact diagonalization of a generalized superoperator \tilde{A} , and it has no relation with the initial state of the system. This technique provides an efficient way for the investigation of the dynamics of the system and not only allow for an efficient numerical analysis, but also, in some cases, for exact algebraic solutions.

The basic idea of this technique is as follows. Instead of solving the ME directly, one can first define two ancillary operators \tilde{A} and $\tilde{\rho}$, which satisfy the following relations

$$\frac{d\tilde{\rho}}{dt} = \tilde{A}\tilde{\rho}, \quad (3)$$

where

$$\tilde{\rho} = (\rho_{1,:}, \rho_{2,:}, \dots, \rho_{d,:})^T. \quad (4)$$

Here d denotes the dimension of the density matrix ρ , $(\dots)^T$ denotes the transpose of (\dots) , and $\rho_{n,:} = [\rho_{n1}, \rho_{n2}, \dots, \rho_{nd}]$ denotes the elements lie in the n th row of ρ . After defining these two ancillary operators, the formal solution of Eq. (3) can be expressed explicitly as

$$\tilde{\rho}(t) = \tilde{U}(t)\tilde{\rho}(0). \quad (5)$$

Since ρ is a $d \times d$ density matrix, the time evolution operator $\tilde{U}(t) = \exp(\tilde{A}t)$ is a $d^2 \times d^2$ matrix, and the initial state of the system $\tilde{\rho}(0)$ is a $d^2 \times 1$ column vector. Moreover, from the definition of $\tilde{\rho}(t)$ one can obtain the equality $\tilde{\rho}_{(i-1)d+j}(t) = \rho_{i,j}(t)$.

Now the key problem is how to obtain the explicit expression of \tilde{A} . The crucial observation to this problem is that the right-hand side of the ME expressed in Eq. (1)

can be divided into the following three terms, i.e.

$$-i[\hat{H}, \rho] + \sum_n \mathcal{L}_n \rho = A\rho + \rho B + \gamma \sum_n c_n \rho c_n^\dagger, \quad (6)$$

where A and B are operators which can be obtained directly from Eqs. (1) and (2) as $A = -i\hat{H} - \gamma \sum_n (c_n^\dagger c_n/2)$, $B = i\hat{H} - \gamma \sum_n (c_n^\dagger c_n/2)$. Hereafter we adopt the conventional notation M_{ij} to denote the element lies in the i th row and j th column of a matrix M , and V_i denotes the i th element of a column vector V . In order to express the ME in forms of $d\tilde{\rho}/dt = \tilde{A}\tilde{\rho}$, we make the following three transformations: $A\rho \mapsto \tilde{A}^{(1)}\tilde{\rho}$, $\rho B \mapsto \tilde{A}^{(2)}\tilde{\rho}$ and $\gamma \sum_n c_n \rho c_n^\dagger \mapsto \tilde{A}^{(3)}\tilde{\rho}$. To ensure the achievement of the first transformation $A\rho \mapsto \tilde{A}^{(1)}\tilde{\rho}$, the equality $(A\rho)_{ij} = (\tilde{A}^{(1)}\tilde{\rho})_{(i-1)d+j}$ must be hold, or equivalently, $\sum_k A_{i,k} \rho_{k,j} = \tilde{A}^{(1)}_{(i-1)d+j,:} \tilde{\rho}$, then after a straightforward algebra, one can obtain $\tilde{A}^{(1)} = A \otimes I$. Similarly, for the second transformation, one can obtain $\tilde{A}^{(2)} = I \otimes B'$, while for the third transformation, one can obtain $\tilde{A}^{(3)} = \gamma \sum_n c_n \otimes c_n^*$. In the above expressions, B' denotes the transposed matrix of B , c_n^* denotes the conjugate of c_n , and I is the $d \times d$ identity matrix. With the help of these results, Eq. (3) becomes

$$\frac{d\tilde{\rho}}{dt} = \sum_{n=1}^3 \tilde{A}^{(n)} \tilde{\rho}. \quad (7)$$

This is just the desired form of the transformed master equation, where the newly defined operator is given by $\tilde{A} = A \otimes I + I \otimes B' + \gamma \sum_n c_n \otimes c_n^*$. Once the explicit form of \tilde{A} has been found, the time evolution operator $\tilde{U}(t) = \exp(\tilde{A}t)$ can be formed and the formal solution of the master equation is obtained, which can be expressed as Eq. (5). To obtain the density operator at arbitrary time t , one only needs to apply the time evolution operator $\tilde{U}(t)$ to the initial state $\tilde{\rho}(0)$ of the system.

Now we try to convert the matrix exponential form of the time evolution operator $\tilde{U}(t) = \exp(\tilde{A}t)$ to the matrix form. For this purpose, we expanded it in terms of the Taylor series as

$$\exp(\tilde{A}t) = \sum_n \frac{(\tilde{A}t)^n}{n!}, \quad (8)$$

where $n!$ denotes the factorial of n . If the $d^2 \times d^2$ matrix \tilde{A} is diagonalizable (\tilde{A} cannot always be diagonalized since it is generally complex and non-Hermitian), i.e., there exists an invertible matrix M that satisfying the relation $M^{-1}\tilde{A}M = \text{diag}(\mathcal{E}_1, \mathcal{E}_2, \dots, \mathcal{E}_{d^2})$, with the diagonal entries \mathcal{E}_k ($k = 1, 2, \dots, d^2$) being the eigenvalues of the operator \tilde{A} , then from Eq. (8) one can obtain

$$M^{-1} \exp(\tilde{A}t) M = \sum_n \frac{(M^{-1}\tilde{A}tM)^n}{n!} = \exp(\mathcal{E}t). \quad (9)$$

From Eq. (9) one can obtain directly that the matrix form of the time evolution operator $\tilde{U}(t)$ is given by

$$\tilde{U}(t) = M \exp(\mathcal{E}t) M^{-1}, \quad (10)$$

where M^{-1} represents the inverse matrix of M , and M is the matrix with the eigenvectors of \tilde{A} as its columns.

From the above analysis, one can see that the achievements of this technique depends solely on the exact diagonalization of the operator \tilde{A} , once \tilde{A} is diagonalized, one can obtain $\tilde{\rho}(t)$ as well as the matrix form of $\rho(t)$ at any time t by applying the time evolution operator $\tilde{U}(t)$, particularly, $\tilde{U}(t)$ has no relation with the initial state $\tilde{\rho}(0)$ of the system, which is economical for performing numerical calculations with different initial states, and this is different from that of the Runge-kutta algorithm.

In the present paper, we first consider effects of dissipative and dephasing environments on state transfer in a spin chain. We assume the quantum state to be transmitted is encoded at the m th spin as $|\varphi_{in}\rangle = \cos(\theta/2)|0\rangle + e^{i\phi}\sin(\theta/2)|1\rangle$ (with $|0\rangle$ and $|1\rangle$ represent the state of spin up and down, respectively), and all the other spins in the chain are initialized to the ground state $|0\rangle$, thus the initial state of the whole system at time $t = 0$ becomes

$$|\psi(0)\rangle = \cos\frac{\theta}{2}|\mathbf{0}\rangle + e^{i\phi}\sin\frac{\theta}{2}|m\rangle, \quad (11)$$

where $|\mathbf{0}\rangle = |00\dots 0\rangle$, $|m\rangle = \sigma_m^+|\mathbf{0}\rangle^{\otimes N}$, $0 \leq \theta \leq \pi$ and $0 \leq \phi \leq 2\pi$ are the relative phase angles. For this type of initial state, the nonzero elements of $\tilde{\rho}(0)$ can be written as

$$\begin{aligned} \tilde{\rho}_{Nm-N+2m-1}(0) &= \sin^2\frac{\theta}{2}, & \tilde{\rho}_{N^2+2N+1}(0) &= \cos^2\frac{\theta}{2}, \\ \tilde{\rho}_{Nm+m}(0) &= \frac{1}{2}e^{i\phi}\sin\theta, & \tilde{\rho}_{N^2+N+m}(0) &= \tilde{\rho}_{Nm+m}^\dagger(0). \end{aligned} \quad (12)$$

Except these four elements, all the other elements of $\tilde{\rho}(0)$ are zero. Here N denotes the length of the chain, and we have used the fact that for initial state $|\psi(0)\rangle$ with the system subjects to dissipative and dephasing environments, its dynamics is completely determined by the time evolution in the zero and single excitation subspace $\mathcal{H}_{0\oplus 1}$ [26, 27, 28, 29], thus it suffices to restrict our attention to the dynamics of $\rho(t)$ in this $(N+1)$ -dimensional subspace spanned by $\{|0\rangle, |1\rangle, |2\rangle, \dots, |N\rangle\}$ which greatly facilitates the following computation process.

To evaluate the extent to which the decoherence affects state transfer in a spin chain, we adopt the concept of fidelity [1] $f = \langle \varphi_{in} | \rho_n(t) | \varphi_{in} \rangle$ as an estimation of the quality of the state transfer from the sender, conventionally named Alice, to the receiver Bob, where $\rho_n(t)$ is the single qubit reduced density matrix. The fidelity measures the overlap between the input state and the output state. In general, if one encodes the state needs to be transmitted at one end of the chain, then after some time t , the state will be recovered at another end of the chain automatically, with however, the fidelity $f < 1$. With elaborately designed structures of the spin chain which is ideally protected from its surrounding environments, the maximum fidelity may reach unity [3, 4, 6, 14, 15]. When subjects to decoherence environments, as can be seen in the following sections, the transfer fidelity cannot reach unity even with elaborately designed spin structures.

In the standard basis $\{|0\rangle, |1\rangle\}$, the single qubit reduced density matrix $\rho_n(t)$ can be obtained by tracing out all other qubits except n from $\rho(t)$ as

$$\rho_n(t) = \begin{pmatrix} 1 - \rho_{nn}(t) & \rho_{N+1,n}(t) \\ \rho_{n,N+1}(t) & \rho_{nn}(t) \end{pmatrix}. \quad (13)$$

Here $\rho_{mn}(t)$ denotes the element lies in the m th row and n th column of $\rho(t)$. Then the state transfer fidelity from the m th qubit to the n th qubit can be computed as

$$f = \cos^2\frac{\theta}{2} - \rho_{nn}\cos\theta + \frac{1}{2}(e^{i\phi}\rho_{N+1,n} + e^{-i\phi}\rho_{n,N+1})\sin\theta. \quad (14)$$

In terms of $\tilde{\rho}(t)$ the elements of $\rho_n(t)$ can be written as

$$\begin{aligned} \rho_{nn}(t) &= \tilde{\rho}_{Nn-N+2n-1}(t), \\ \rho_{n,N+1}(t) &= \tilde{\rho}_{Nn+n}(t), \\ \rho_{N+1,n}(t) &= \tilde{\rho}_{N^2+N+n}(t). \end{aligned} \quad (15)$$

The explicit form of $\tilde{\rho}_{Nn-N+2n-1}(t)$, $\tilde{\rho}_{Nn+n}(t)$ and $\tilde{\rho}_{N^2+N+n}(t)$ can be expressed as

$$\begin{aligned} \tilde{\rho}_{Nn-N+2n-1} &= \tilde{U}_{Nn-N+2n-1, Nm-N+2m-1} \sin^2\frac{\theta}{2} \\ &\quad + \tilde{U}_{Nn-N+2n-1, N^2+2N+1} \cos^2\frac{\theta}{2} \\ &\quad + \frac{1}{2}(\tilde{U}_{Nn-N+2n-1, Nm+m} e^{i\phi} \\ &\quad + \tilde{U}_{Nn-N+2n-1, N^2+N+m} e^{-i\phi}) \sin\theta, \\ \tilde{\rho}_{Nn+n} &= \tilde{U}_{Nn+n, Nm-N+2m-1} \sin^2\frac{\theta}{2} \\ &\quad + \tilde{U}_{Nn+n, N^2+2N+1} \cos^2\frac{\theta}{2} \\ &\quad + \frac{1}{2}(\tilde{U}_{Nn+n, Nm+m} e^{i\phi} \\ &\quad + \tilde{U}_{Nn+n, N^2+N+m} e^{-i\phi}) \sin\theta, \\ \tilde{\rho}_{N^2+N+n} &= \tilde{U}_{N^2+N+n, Nm-N+2m-1} \sin^2\frac{\theta}{2} \\ &\quad + \tilde{U}_{N^2+N+n, N^2+2N+1} \cos^2\frac{\theta}{2} \\ &\quad + \frac{1}{2}(\tilde{U}_{N^2+N+n, Nm+m} e^{i\phi} \\ &\quad + \tilde{U}_{N^2+N+n, N^2+N+m} e^{-i\phi}) \sin\theta. \end{aligned} \quad (16)$$

Substituting these results into Eq. (14), one can obtain the explicit form of the state transfer fidelity. Particularly, when $\theta = \pi$, we obtain the transfer fidelity of an excitation as $f = \langle 1 | \rho_n(t) | 1 \rangle = \tilde{U}_{Nn-N+2n-1, Nm-N+2m-1}$. On the other hand, in order to assess the efficiency of the quantum spin channel of interest, it is more beneficial to calculate the average fidelity (the fidelity averaged over all pure input states in the Bloch sphere) $F = \frac{1}{4\pi} \int f d\Omega =$

$\frac{1}{4\pi} \int_0^\pi \int_0^{2\pi} f \sin \theta d\theta d\phi$ [1], which can be computed as

$$F = \frac{\tilde{U}_{N^2+N+n, N^2+N+m} + \tilde{U}_{Nn+n, Nm+m}}{6} + \frac{\tilde{U}_{Nn-N+2n-1, Nm-N+2m-1}}{6} - \frac{\tilde{U}_{Nn-N+2n-1, N^2+2N+1}}{6} + \frac{1}{2}. \quad (17)$$

From the above equation one can see that the average fidelity F is solely determined by the time evolution operator $\tilde{U}(t)$. In a previous work [43], Bowdrey et al. have also derived a similar expression for average fidelity in the form of unitary (or anti-unitary) operators. Moreover, Eq. (17) can be simplified under certain special conditions. For example, if one chooses the correlated spin chain Hamiltonian of the considered quantum system as $\hat{H} = \sum_n [J_{n,n+1}(\sigma_n^x \sigma_{n+1}^x + \sigma_n^y \sigma_{n+1}^y) + \Delta_{n,n+1} \sigma_n^z \sigma_{n+1}^z + B_n \sigma_n^z]$, then it is direct to show that the last column of \hat{H} can be written as $\hat{H}_{:,d} = (0, 0, \dots, 0, c)^T$ in the standard basis, where d is the dimension of \hat{H} , $c = \sum_n (\Delta_{n,n+1} + B_n)$ is a nonzero number. Combination of these results with the expression of the operator $\tilde{A} = A \otimes I + I \otimes B' + \gamma \sum_n c_n \otimes c_n^*$, one can show that the last column of \tilde{A} has the form $\tilde{A}_{:,d^2} = (0, 0, \dots, 0)^T$, thus by adopting the Taylor series expansion of the time evolution operator $\tilde{U}(t) = \exp(\tilde{A}t)$, one can compute the last column of $\tilde{U}(t)$ as $\tilde{U}_{:,d^2} = (0, 0, \dots, 0, 1)^T$ (note that this expression is valid for all subspaces, when restricted to the subspace $\mathcal{H}_{0\oplus 1}$, it holds true even for the system Hamiltonian with inhomogeneous x and y components), this gives rise to a simplification of Eq. (17) as

$$F = \frac{\tilde{U}_{N^2+N+n, N^2+N+m} + \tilde{U}_{Nn+n, Nm+m}}{6} + \frac{\tilde{U}_{Nn-N+2n-1, Nm-N+2m-1}}{6} + \frac{1}{2}. \quad (18)$$

Eqs. (17) and (18) are the main results we obtained in this paper, which will be used in the latter discussion of quantum state transfer when an explicit form of the spin chain Hamiltonian is given. Particularly, for the mirror-symmetric Hamiltonian \hat{H}_m (by mirror symmetry, we mean that the interaction Hamiltonian of the spin chain has symmetric coupling strengths about the centre qubit or the centre link, i.e., the coupling strength $J_{m,n} = J_{N-m+1, N-n+1}$) we have $\tilde{U}_{N^2+N+n, N^2+N+m} = \tilde{U}_{Nn+n, Nm+m}^\dagger$. In the absence of decoherence environments (i.e., $\gamma = 0$), this yields $\tilde{U}_{N^2+N+n, N^2+N+m} + \tilde{U}_{Nn+n, Nm+m} = 2\text{Re}\{\langle n | \exp(-i\hat{H}_m t) | m \rangle\} = 2|\langle n | \exp(-i\hat{H}_m t) | m \rangle| \cos \alpha$ and $\tilde{U}_{Nn-N+2n-1, Nm-N+2m-1} = |\langle n | \exp(-i\hat{H}_m t) | m \rangle|^2$, where $\alpha = \arg\{\langle n | \exp(-i\hat{H}_m t) | m \rangle\}$ denotes the argument of the complex number $\langle n | \exp(-i\hat{H}_m t) | m \rangle$. Clearly, this is just that of Eq. (6) in Ref. [1], which describes average fidelity in the non-disturbed case.

3 State transfer in decoherence spin channels

Recently, intense research efforts has been devoted to the interacting spin systems which were proposed as potential candidates to simulate the relation between qubits in a quantum computer [44]. This choice is due to the fact that such systems can be easily manipulated (e.g., by tunneling potentials or energy bias) and scaled up to large registers. In the present paper, we investigate state transfer in this kind of system, with the addition of the presence of the dissipative and dephasing environments. We concentrated on the spin channel with fixed but different coupling strengths between neighboring qubits, with the Hamiltonian given by

$$\hat{H} = \sum_{n=1}^{N-1} \frac{J_{n,n+1}}{2} (\sigma_n^x \sigma_{n+1}^x + \sigma_n^y \sigma_{n+1}^y), \quad (19)$$

where σ_n^α ($\alpha = x, y, z$) are the usual Pauli operators acting on the n th spin, $J_{n,n+1} = \lambda \sqrt{n(N-n)}$ is the modulated exchange coupling strength, and λ is a scaling constant. This Hamiltonian is identical to the representation of the Hamiltonian of a fictitious spin $S = (N-1)/2$ particle: $\hat{H}_S = \lambda S_x$, where S_x is its angular momentum operator in the x -direction.

For this modulated spin chain, it has been shown that one can achieve perfect state transfer between the input node n and the output node $N-n+1$ after a time $t_0 = \pi/2\lambda$ and at intervals of π/λ thereafter in the absence of decoherence environment, i.e., when $t = (2k-1)\pi/2\lambda$, $k = \{1, 2, \dots\}$, the transfer fidelity reaches unity [3,4]. When the decoherence is present, however, this ideal communication channel may be destroyed. To show that this is so, we consider effects of dissipative and dephasing environments on quantum state transfer from one end of the chain to another. The average fidelity can be obtained directly from Eq. (18) by replacing (m, n) with $(1, N)$. Moreover, since the Hamiltonian \hat{H} expressed in Eq. (19) is mirror symmetric, we have $\tilde{U}_{N^2+2N, N^2+N+1} = \tilde{U}_{N^2+N, N+1}^\dagger$, thus the average fidelity can be rewritten as

$$F = \frac{|\tilde{U}_{N^2+2N, N^2+N+1}| \cos \alpha}{3} + \frac{\tilde{U}_{N^2+N-1, 1}}{6} + \frac{1}{2}. \quad (20)$$

Physically, one can maximize the average fidelity F by performing a phase flip operation or applying an external magnetic field along the z axis such that α is a multiple of 2π . Furthermore, for the case of dissipative environment one can show that $\tilde{U}_{N^2+N-1, 1} = |\tilde{U}_{N^2+2N, N^2+N+1}|^2$, thus the expression of the average fidelity F is very similar to that of Eq. (6) in Ref. [1], which describes the average fidelity in the non-disturbed case. However, for the case of dephasing environment, one cannot obtain such a simple relation. Except this, there exists another difference between the dissipative and the dephasing environments which may be useful in the following discussion. To demonstrate this explicitly, it is illuminating to rewrite the ancillary operator $\tilde{A} = A \otimes I + I \otimes B' + \gamma \sum_n c_n \otimes c_n^*$ as $\tilde{A} = \tilde{A}(1) + \tilde{A}(2)$, where $\tilde{A}(1) = -i(\hat{H} \otimes I - I \otimes \hat{H}')$ and

$\tilde{A}(2) = \gamma \sum_n \{c_n \otimes c_n^* - \frac{1}{2}[(c_n^\dagger c_n) \otimes I + I \otimes (c_n^\dagger c_n)']\}$, then for the case of dissipative environment, one can show directly that $\tilde{A}(1)$ and $\tilde{A}(2)$ commutes with each other, i.e., $[\tilde{A}(1), \tilde{A}(2)] = 0$, while for the case of dephasing environment, one still cannot obtain this commutation relation.

As a heuristic analysis, we first consider dissipative effects on fidelity of quantum state transfer from one end of the chain to another at time $t_0 = (2k-1)\pi/2\lambda$. This choice of time t_0 is based on the fact that for weak system-environment coupling strength γ , the difference between t_0 and the critical time t_c at which the transfer fidelity attains its maximum value is minimal (e.g., for $N = 2$ and $\gamma = 0.1$, the deviation for transfer fidelity of an excitation at time t_0 is about 0.2496% from that at time t_c), particularly, for large N and small γ , this difference can even be neglected (see the inset of Fig. 1). For this kind of decoherence mode, from the commutation relation $[\tilde{A}(1), \tilde{A}(2)] = 0$ one can find that the time evolution operator $\tilde{U}(t) = \exp(\tilde{A}t)$ can be rewritten as $\tilde{U}(t) = \exp[\tilde{A}(1)t] \exp[\tilde{A}(2)t]$. For the first term, from the equality $(A \otimes L)(B \otimes M) = AB \otimes LM$ and the Taylor series expansion of it one can obtain $\exp[\tilde{A}(1)t] = [\exp(-it\hat{H}) \otimes I][I \otimes \exp(it\hat{H}')]$. When restricted to the zero and single excitation subspace $\mathcal{H}_{0\oplus 1}$, the eigenvalues and the corresponding eigenvectors of \hat{H} can be readily obtained as [45]

$$\begin{aligned} \mathcal{E}_0 &= 0, & \mathcal{E}_k &= -(N-2k+1)\lambda, \\ |\psi_0\rangle &= |\mathbf{0}\rangle, & |\psi_k\rangle &= \sum_{n=1}^N c_{k,n} |n\rangle, \end{aligned} \quad (21)$$

where $k = \{1, 2, \dots, N\}$, and the coefficient $c_{k,n}$ is given by the following recursion relations

$$\begin{aligned} c_{1,1} &= \frac{1}{\sqrt{2^{(N-1)}}}, & c_{k,1} &= (-1)^{k+1} c_{1,k}, \\ c_{k,n} &= \frac{\mathcal{E}_k c_{k,n-1} - \sqrt{(n-2)(N-n+2)} c_{k,n-2}}{\sqrt{(n-1)(N-n+1)}} \quad (n \geq 2). \end{aligned} \quad (22)$$

Then $\exp[\tilde{A}(1)t_0]$ can be obtained analytically (for the ease of presentation, we omitted its explicit expression since this provides no new insights on the system), and the $(N^2 + N - 1)$ -th row of it is $[1, 0, 0, \dots, 0]$, while the $(N^2 + 2N)$ -th row of it is $[0, \dots, 0, i^{(N-1)(2k-1)}, 0, \dots, 0]$, with the only nonzero element $i^{(N-1)(2k-1)}$ locating at the $(N^2 + N + 1)$ -th column.

On the other hand, the eigenvalues and the eigenvectors of $\tilde{A}(2)$ can also be obtained analytically, the results are expressed as follows

$$\begin{aligned} E &= \gamma(0, c_1, c_1, \dots, c_1, c_2), \\ M &= \begin{pmatrix} g & & & & \\ & g & & & \\ & & \ddots & & \\ & & & \ddots & \\ 1 & d & d & \dots & d \end{pmatrix}, \end{aligned} \quad (23)$$

where the elements of the $(N+1)^2$ -dimensional row vector E are eigenvalues of $\tilde{A}(2)$, M is the $[(N+1)^2 \times (N+1)^2]$ -dimensional matrix with eigenvectors of $\tilde{A}(2)$ as its columns. Except the parameters 1, d and g , all the other elements in the matrix M are zero. The explicit form of c_1 , c_2 , d and g are given by

$c_1 = -(\underbrace{1, 1, \dots, 1}_N, 0.5)$, $c_2 = -(\underbrace{0.5, 0.5, \dots, 0.5}_N)$, $d = (-1/\sqrt{2}, \underbrace{0, 0, \dots, 0}_{N+1})$, $g = \text{diag}(1/\sqrt{2}, \underbrace{1, 1, \dots, 1}_{N+1})$.

$$\begin{aligned} c_1 &= -(\underbrace{1, 1, \dots, 1}_N, 0.5), & c_2 &= -(\underbrace{0.5, 0.5, \dots, 0.5}_N), \\ d &= (-1/\sqrt{2}, \underbrace{0, 0, \dots, 0}_{N+1}), & g &= \text{diag}(1/\sqrt{2}, \underbrace{1, 1, \dots, 1}_{N+1}). \end{aligned} \quad (24)$$

Thus the analytical form of $\exp[\tilde{A}(2)t_0]$ can also be obtained. The first and the $(N^2 + N + 1)$ -th column of it can be written explicitly as $[e^{-\gamma t_0}, 0, \dots, 0, 1 - e^{-\gamma t_0}]^T$ and $[0, \dots, 0, e^{-\gamma t_0/2}, 0, \dots, 0]^T$, with the only nonzero element $e^{-\gamma t_0/2}$ locating at the $(N^2 + N + 1)$ -th row.

From the above analytical results, one can obtain the transfer fidelity of an excitation and the average fidelity at time $t_0 = (2k-1)\pi/2\lambda$ as

$$\begin{aligned} f(t_0) &= e^{-\gamma t_0}, \\ F(t_0) &= \frac{e^{-\gamma t_0/2} \cos \alpha}{3} + \frac{e^{-\gamma t_0}}{6} + \frac{1}{2}, \end{aligned} \quad (25)$$

where $\cos \alpha = \text{Re}[i^{(N-1)(2k-1)}]$. From the above equation one can see that when the system subjects to dissipative environment, the transfer fidelity $f(t_0)$ of an excitation is independent of the spin chain length N . For fixed t_0 , it will exponentially decay with the increase of the decoherence rate γ , while for fixed γ , it will exponentially decay with the increase of t_0 (this phenomenon may be understood physically from that fact that we have assumed the dissipation acts independently and equally on each spin, and since there is a single excitation, the survival probability of this excitation should be an exponential function of the time t_0). The average fidelity $F(t_0)$ is, however, dependent on the spin chain length N due to the existence of the phase factor $\cos \alpha$. As can be found from Eq. (25), $F(t_0)$ displays three different dynamical patterns corresponding to $N = 4r + 1$, $N = 4r - 1$ and $N = 2r$ ($r = 1, 2, \dots$). For the latter two patterns of N , one needs to perform a phase flip operation at the end spin belonging to the receiver [4] or apply an external magnetic field to spins of the system [1] to maximize the average fidelity (after these operations, the average fidelity at time t_0 is also independent of the spin chain length N and will display behaviors completely the same as that depicted by the red diamonds in the bottom panel of Fig. 1). If there are no additional operations are performed, from Fig. 1 one can observe that only when $N = 4r + 1$ (or equivalently, $N - 1$ to be divisible by 4) can the quantum spin channel may be superior to its classical counterpart, for which the highest fidelity for transmission of a quantum state is $2/3$ [46].

For arbitrary evolution time t , after a tedious computation, we obtain the state transfer fidelity of an excitation

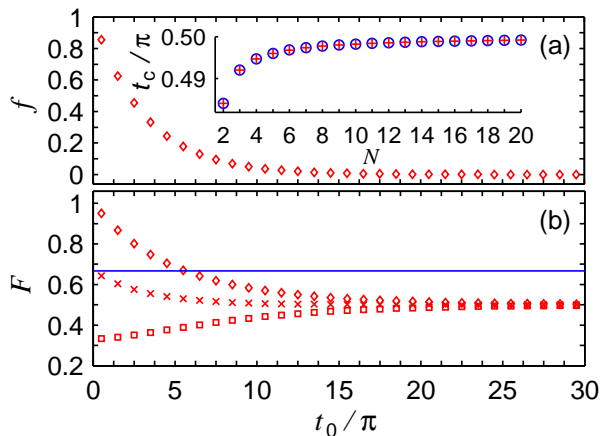


Fig. 1. (Color online) Transfer fidelity of an excitation (a) and the average fidelity (b) versus the rescaled time $t_0/\pi = (2k-1)/2$ ($k = 1, 2, \dots$) with the system subjects to dissipative environment, where the decoherence rate and the scaling constant are given by $\gamma = 0.1$ and $\lambda = 1$. In (b), the plots from top to bottom correspond to $N = 4r + 1$, $N = 2r$ and $N = 4r - 1$ ($r = 1, 2, \dots$), with the straight line at $F = 2/3$ shows the highest fidelity for classical transmission of a quantum state. The inset in (a) shows t_c/π versus N , t_c is the critical time at which the transfer fidelity of an excitation (blue circles) and the average fidelity (red plus signs) attain their maxima.

and the average fidelity analytically as

$$f(t) = e^{-\gamma t} \sin^{2(N-1)} \lambda t,$$

$$F(t) = \frac{e^{-\gamma t/2} \sin^{N-1}(\lambda t) \cos \alpha}{3} + \frac{e^{-\gamma t} \sin^{2(N-1)} \lambda t}{6} + \frac{1}{2}. \quad (26)$$

From the above equation one can see that under the detrimental influence of dissipative environment, both $f(t)$ and $F(t)$ behave as suppressed oscillations as the time evolves. Moreover, the decay of the average fidelity $F(t)$ displays three different patterns mediated by a phase factor $\cos \alpha = \text{Re}[i^{(N-1)(2k-1)}]$.

From Eq. (26) one can also see that there exists a region in which the dissipative spin channel is superior to its classical counterpart. This region can be obtained analytically by solving the nonlinear equation $F(t_c) > 2/3$, which gives rise to $\gamma < \ln(2 \cos^2 \alpha + 2 \cos \alpha \sqrt{1 + \cos^2 \alpha} + 1)/t_c$. If we choose $\cos \alpha = 1$ and $t_c \simeq t_0 = \pi/2$ (i.e., $\lambda = 1$), then we have $\gamma < 1.122$, and this result is independent of the spin chain length N .

When the system subjects to dephasing environment, however, one cannot obtain an analytical result as that of the dissipative environment because $[\tilde{A}(1), \tilde{A}(2)] \neq 0$, so we resort to numerical techniques. The typical results are shown in Fig. 2, from which one can see that the transfer fidelity of an excitation $f(t_0)$ also decays with the increase of t_0 , however, when $t_0 \rightarrow \infty$, $f(t_0)$ arrives at a nonzero value $f(t_0 \rightarrow \infty) = 1/N$, and this is different from that of the dissipative environment, in which $f(t_0)$ decays to zero asymptotically. There is another difference exists, namely, for any fixed decoherence rate γ , $f(t_0)$ decreases with the

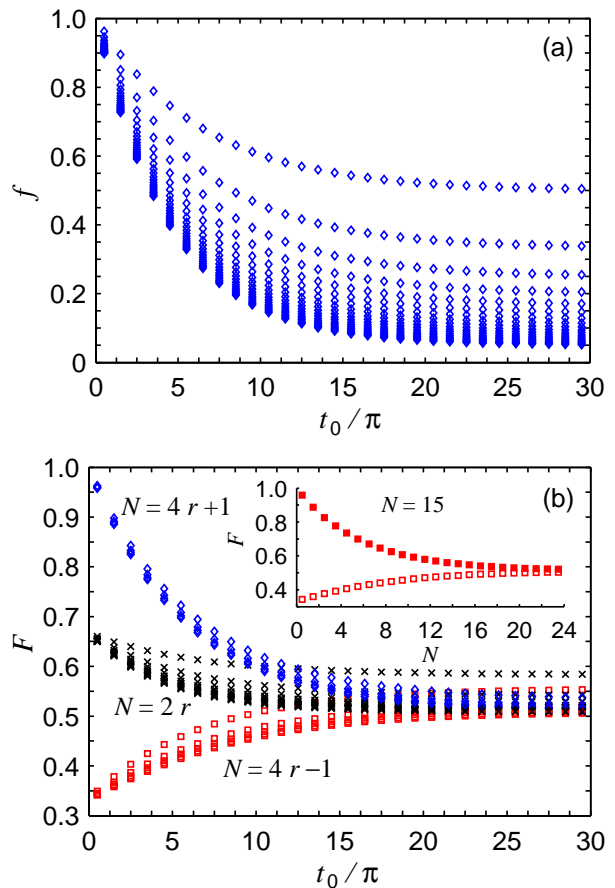


Fig. 2. (Color online) Transfer fidelity of an excitation (a) and the average fidelity (b) versus the rescaled time $t_0/\pi = (2k-1)/2$ ($k = 1, 2, \dots$) with the system subjects to dephasing environment. Here the decoherence rate and the scaling constant are given by $\gamma = 0.1$ and $\lambda = 1$. For (a), the plots from top to bottom correspond to $N = 2$ to $N = 20$. For (b), the blue diamonds from top to bottom correspond to $r = 1$ to $r = 4$, the black crosses from top to bottom correspond to $r = 1$ to $r = 10$, and the red squares from top to bottom correspond to $r = 1$ to $r = 5$. The inset in (b) is an exemplified figure plotted for the comparison of the average fidelity F before (hollow squares) and after (solid squares) the phase shift caused by the factor $\cos \alpha$ being corrected.

increase of N for the case of dephasing environment, which is disadvantageous for long distance quantum communication. The average fidelity $F(t_0)$ is also dependent on the spin chain length, and it displays three different patterns for different kinds of N . As can be seen from Fig. 2b, only for the case of $N = 4r + 1$ ($r = 1, 2, \dots$) can the quantum spin channel may be superior to its classical counterpart if no other performance have been made. When $t_0 \rightarrow \infty$, the average fidelity also arrives at a constant value which is also dependent on N , and can be computed analytically as $F(t_0 \rightarrow \infty) = 1/6N + 1/2$.

For fixed spin chain length N and critical time t_c , there also exists a critical decoherence rate γ_c before which the dephasing channel is superior to any classical communication channel, for which can only ensure transmission of

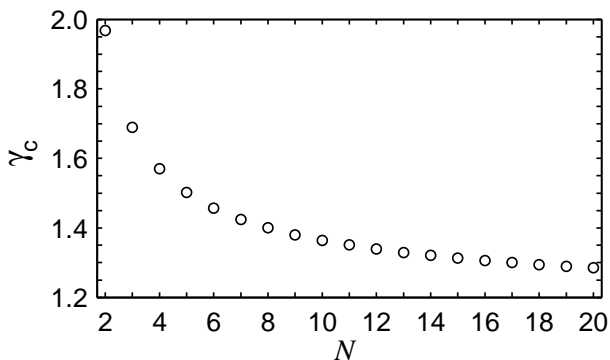


Fig. 3. Critical decoherence rate γ_c versus N with the system subjects to dephasing environment, where the scaling constant λ has been chosen to be 1, and the phase shift for $N = 4r - 1$ and $N = 2r$ has been assumed to be eliminated.

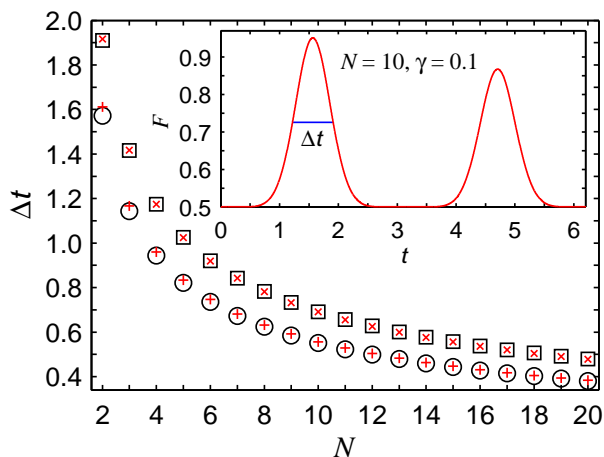


Fig. 4. (Color online) FWHM Δt of the first oscillation versus N with $\gamma = 0.1$ and $\lambda = 1$. The black squares and circles show Δt corresponds to the case of the transfer fidelity of an excitation and the average fidelity with the system subjects to dissipative environment, while the red crosses and plus signs show Δt corresponds to those with the system subjects to dephasing environment. Moreover, the average fidelity was plotted with the phase shift being corrected, and the inset is a schematic picture (with the system subjects to dissipative environment) annotating the meaning of the FWHM.

a quantum state with the highest fidelity $2/3$ [46]. The typical plots of γ_c versus N with scaling constant $\lambda = 1$ is shown in Fig. 3, where we have assumed that the phase shift caused by the factor $\cos \alpha$ is eliminated by choosing $\cos \alpha = 1$ for the cases of $N = 4r - 1$ and $N = 2r$. From this figure one can see that γ_c decreases with the increase of N , this puts another constraint on this spin channel for long distance quantum communication because for large N , one needs to reduce the mutual interaction between the system of interest and its surrounding environment in order to obtain a reliable transfer fidelity, and in general, this is not an easy task in real experiments.

From the aforementioned analysis one can see that increasing the decoherence rate γ or the spin chain length N

always introduces stringent constraints on the spin channel for long distance quantum communication. In the following, we discuss another serious constraint imposed by the dissipative and dephasing environments on the spin channel. For this purpose, we examine full width at half maximum (FWHM) of the first oscillation describing the dynamics of the fidelity of an excitation as well as the average fidelity and we denote it as $\Delta t = |t_2 - t_1|$, with $f(t_1) = f(t_2) = f_{max}/2$ and $F(t_1) = F(t_2) = F_{max}/2$. For the case of dissipative environment, from Eq. (26) one can obtain the following two relations

$$\begin{aligned} e^{-\gamma t} \sin^{2(N-1)} \lambda t &= f_{max}/2, \\ e^{-\gamma t/2} \sin^{N-1} \lambda t &= \sqrt{3F_{max} - 3 + \cos^2 \alpha} - \cos \alpha, \end{aligned} \quad (27)$$

where for transfer fidelity of an excitation, (t_1, t_2) can be obtained by solving the nonlinear equation expressed in the first line of Eq. (27), and for the average fidelity, (t_1, t_2) can be obtained by solving the second equation expressed in Eq. (27). The maximum value of f_{max} and F_{max} can be obtained directly from Eq. (26).

For the case of dephasing environment, however, one cannot obtain a result similar to that of Eq. (27), thus we resort to numerical methods. The exemplified plots are shown in Fig. 4, where for the case of average fidelity, we have chosen $\cos \alpha = 1$. From this figure one can see that the curves exhibit nearly the same behaviors for both of the decoherence scenarios. With the increase of the spin channel length N , the FWHM Δt decreases one by one, which implies that the peak of the wave becomes steeper and narrow with the increase of N . This puts a stringent limitation on the time when the measurement must be performed by the receiver Bob, because for large N , when the transmitted state arrives at the destination qubits, Bob should make measurements on the qubits at the instant time of t_c as quickly as possible, otherwise, even a minor deviation of measurement time from t_c would lead to a great inaccuracy to the transmitted state.

We now turn to investigate quantum state transfer in another spin channel proposed by Shi et al. [6], the Hamiltonian of the system has the similar form as that expressed in Eq. (19), with however, the coupling strength between neighboring spins given by

$$J_{n,n+1} = \begin{cases} \lambda \sqrt{n(N-n)} & (n \in \text{even}), \\ \lambda \sqrt{(n+2k)(N-n+2k)} & (n \in \text{odd}). \end{cases} \quad (28)$$

Here $k = \{0, 1, 2, \dots\}$, and λ is still a scaling constant. This Hamiltonian is the same as that of Eq. (19) when $k = 0$. For other cases of k and $N \in \text{even}$, it can be used to achieve perfect state transfer from the first node to the last node at time $t_0 = \pi/2\lambda$ and periodically returns there at regular time intervals of π/λ in the absence of decoherence environment (for the special case of $N = 2$, perfect state transfer can also be achieved at time $t = \pi/(4k+2)\lambda + \pi r/(2k+1)\lambda$, $r = \{0, 1, 2, \dots\}$). Here we discuss how the dissipative and dephasing environments affect quantum state transfer in this spin channel. Since the case of $k = 0$ has been discussed in the above section,

here we concentrated only on dynamics of state transfer fidelity at time $t_0 = (2k - 1)\pi/2\lambda$ for the case of $k \geq 1$. The eigenvalues and the eigenvectors of the corresponding Hamiltonian have been obtained in Ref. [6], and this enables an analytical analysis for the case of dissipative environment, while for dephasing environment, we also resort to numerical analysis. Our results revealed that for both of the decoherence modes, the transfer fidelity of an excitation and the average fidelity at time t_0 for $k \geq 1$ show completely the same behaviors as that of $k = 0$ and $N \in \text{even}$, thus the region in which this spin channel is superior to any classical communication channel is also the same as that of $k = 0$ and $N \in \text{even}$. However, for any fixed $N \in \text{even}$, the FWHM Δt becomes narrower and narrower with the increase of k , thus by the same argument as made in the previous section, we suggest that in practice, one can choose $k = 0$ in order to minimize the deviations from the transmitted state introduced by the measurement process.

Moreover, for the special case of $N = 2$ at arbitrary evolution time t , the transfer fidelity of an excitation and the average fidelity with the system subjects to dissipative environment can be obtained analytically as $f(t) = e^{-\gamma t} \sin^2[(2k + 1)\lambda t]$ and $F(t) = e^{-\gamma t} \sin^2[(2k + 1)\lambda t]/6 + 1/2$. For the case of the system subjects to dephasing environment, again due to the fact that $[\hat{A}(1), \hat{A}(2)] \neq 0$, one cannot obtain an analytical result of the state transfer fidelity.

4 Entanglement distribution and creation in decoherence spin channels

From the above discussion one can see that both the dissipative and dephasing environments have severely detrimental effects on fidelity of quantum state transfer. How these decoherence modes affect other dynamical processes of a quantum system. As an answer to this question, in this section we investigate decoherence effects on entanglement distribution and creation. We first see entanglement distribution between two distant parties through the dissipative and dephasing spin channels. To assess the extent to which these decoherence environments affect entanglement distribution, we assume the entangled state $|\psi\rangle = (|01\rangle + |10\rangle)/\sqrt{2}$ is initially prepared between a non-interacting qubit NI and the first qubit A of the chain, then after some time t , the entanglement may be established between NI and the N th qubit B. The overall Hamiltonian of the system can be written as $\hat{H}_{\text{over}} = I_2 \otimes \hat{H}$ (I_2 denotes the 2×2 identity matrix). To assess the amount of the pairwise entanglement at different instants of time, we adopt the concurrence, a function introduced by Wootters [47], equals to 1 for maximally entangled states and zero for separable states, defined as $C = \max\{0, \lambda_1 - \lambda_2 - \lambda_3 - \lambda_4\}$, where λ_i ($i = 1, 2, 3, 4$) are the square roots of the eigenvalues of the matrix $R = \rho_{mn}(\sigma_m^y \otimes \sigma_n^y) \rho_{mn}^*(\sigma_m^y \otimes \sigma_n^y)$ (ρ_{mn} is the two-qubit reduced density matrix). Then after a similar numerical analysis as performed in Section 3, we obtained entanglement dynamics of the system. The re-

sults revealed two remarkable features (see Fig. 5). First, for both of the decoherence modes, the pairwise entanglement between the non-interacting qubit NI and the last qubit B measured by the concurrence $C_{\text{NI,B}}(t)$ display completely the same behaviors, i.e., they both behave as suppressed fluctuations as the time t evolves, and the entanglement may experience sudden death [48] during certain intervals of the evolution time (see the inset in the top panel of Fig. 5). Second, for any fixed decoherence rate γ , the maximum value of $C_{\text{NI,B}}(t)$ decreases smoothly with the increase of the spin chain length N , and the critical time t_c at which the concurrence $C_{\text{NI,B}}(t)$ attains its maximum value still does not locate at $t_0 = \pi/2\lambda$ (at this point, the concurrence can be obtained analytically as $C_{\text{NI,B}}(t_0) = e^{-\gamma t_0}$, which is independent of N). t_c increases as N increases, and when $N \rightarrow \infty$, t_c approaches its asymptotic value $\pi/2\lambda$, which is the same as that of t_0 . This implies that even for very large N , one can still obtain substantial concurrence $C_{\text{NI,B}}(t_c) = e^{-\gamma\pi/2\lambda}$ (it is not difficult to understand this phenomenon, because the scaling for large N also involves increasing the coupling strengths between the neighboring spins for we have chosen $J_{n,n+1} = \lambda\sqrt{n(N-n)}$).

Next we turn to investigate how the dissipative and dephasing environments affect the creation of entanglement in spin networks. For this purpose, we consider the multi-arm structure $M(N_1, N_2, N_A)$ of the XX spin chain Hamiltonian (19) with the addition of the exchange couplings between the hub site and its nearest-neighbor output sites satisfy the branching rule [10, 49]. Here N_1 and N_2 denote the number of sites in the input and output arms, respectively, and N_A denotes the number of output arms (see the inset in the top panel of Fig. 6). It has been shown that in the absence of decoherence environment, this structure can be employed to create multi-qubit entangled W state [10, 50] at the ends of the outgoing arms. When the system is subjected to the decoherence environment, however, the case may be different.

When the quantum system subjects to dissipative environment, our numerical results revealed that the concurrence C (here C measures amount of the created pairwise entanglement between arbitrary two end nodes of the output arms) is determined by two numbers $N = N_1 + N_2 + 1$ and N_A . For any fixed N_A and decoherence rate γ , the maximum value of the concurrence decreases with the increase of N . This is different from that of the ideal case (i.e., $\gamma = 0$), for which the concurrence has no relation with N [10, 49]. Moreover, similar to the case of entanglement distribution in a spin chain, the critical time t_c at which the concurrence attains its maximum value is also slightly different from $t_0 = \pi/2\lambda$ for small values of N (see the top panel of Fig. 6), while t_c is nearly independent of N_A . In the limit of $N \rightarrow \infty$, however, $t_c \rightarrow t_0 = \pi/2\lambda$, at which the concurrence can be obtained explicitly as $C(t_c) = 2e^{-(\gamma\pi/2\lambda)}/N_A$.

When the system subjects to dephasing environment, however, our numerical results revealed that the concurrence $C(t)$ is dependent on N_1 , N_2 and N_A , which is different from that of the dissipative environment. For fixed

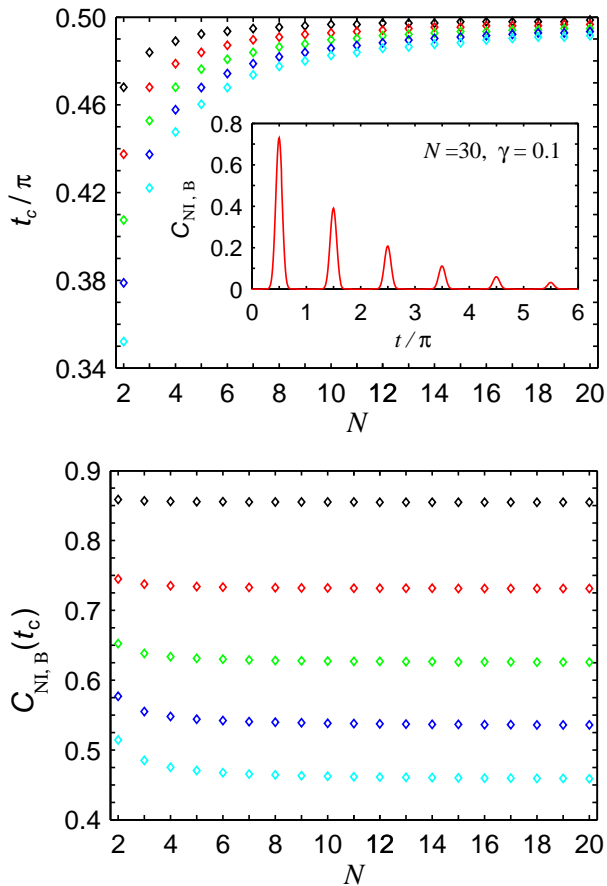


Fig. 5. (Color online) Rescaled critical time t_c/π and the maximum concurrence $C_{\text{NI,B}}(t_c)$ versus N with the system subjects to dissipative or dephasing environment. For every plot, the diamonds from top to bottom correspond to $\gamma = 0.1, 0.2, 0.3, 0.4, 0.5$. The inset in the top panel shows dynamics of the concurrence $C_{\text{NI,B}}$ versus t/π . The other parameter values are given by $\gamma = 0.1$ and $\lambda = 1$.

$N = N_1 + N_2 + 1$, the maximum value of $C(t)$ decreases with the increase of N_2 , thus in order to minimize the detrimental effects of dephasing environment on entanglement creation, one can design the spin structure with the number of sites in each output arm as $N_2 = 1$. Moreover, as can be seen from Fig. 6, when the system subjects to dephasing environment, the critical time t_c at which the concurrence attains its maximum approaches the asymptotic value $\pi/2\lambda$ more quickly than that for the dissipative environment, and the detrimental effects of the dissipative environment seems to be more severe than that of the dephasing environment under the condition of the same decoherence rate γ .

5 Summary and discussion

In the present paper, by exact diagonalization of a generalized superoperator for solving the master equation, we investigated quantum state transfer, as well as entanglement distribution and creation through the dissipative and

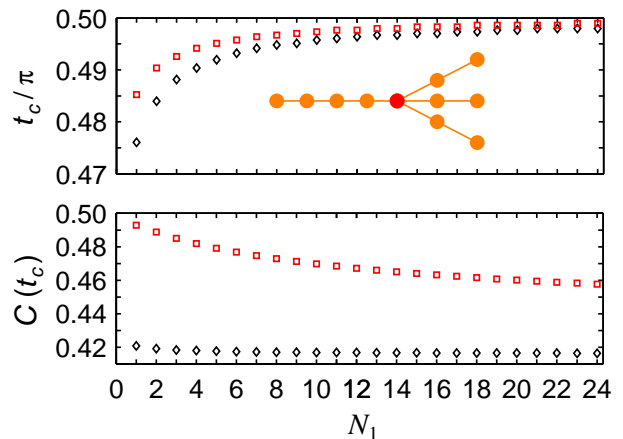


Fig. 6. (Color online) Rescaled critical time t_c/π and the maximum concurrence $C(t_c)$ versus N_1 with the system subjects to dissipative (black diamonds) and dephasing (red squares) environments. The other parameters for the plots are $N_2 = 1$, $N_A = 3$, $\gamma = 0.3$ and $\lambda = 1$. The inset in the top panel is an exemplified multiarm structure of the spin network with the solid red circle denotes the hub, and the number of sites in the input and output arms are given by $N_1 = 4$, $N_2 = 2$, while the number of output arms is $N_A = 3$.

dephasing spin channels, aimed at revealing the extent to which these decoherence environments affect various QIP tasks. We focused on several interaction-modulated spin networks which may serve as perfect spin channels in the absence of decoherence, and gave an analytical analysis for the case of dissipative environment, and numerical analysis for the case of dephasing environment. The results revealed three general conclusions. The first is that these two decoherence environments always lead to suppression of the state transfer fidelity, as well as the amount of the distributed and created pairwise entanglement, particularly, this suppression increases with the increase of the decoherence rate γ . The second is that the detrimental effects of the dissipative environment are more severe than that of the dephasing environment under the condition of the same decoherence rate γ . The third is that the critical time t_c at which the transfer fidelity and the concurrence attain their maxima increases with the increase of N , and when $N \rightarrow \infty$, it approaches the asymptotic value $t_0 = \pi/2\lambda$.

For the case of state transfer, the results also revealed that for fixed γ , the transfer fidelity of an excitation $f(t_0)$ decreases with the increase of t_0 , while the average fidelity $F(t_0)$ displays three different patterns corresponding to the chain length $N = 4r + 1$, $N = 4r - 1$ and $N = 2r$, and only when $N = 4r + 1$ can the spin channel superior to all of its classical counterpart if there are no additional operations being performed. Besides this, when the system subjects to dissipative environment, $f(t_0)$ is independent of N , while for each pattern N , $F(t_0)$ is independent of r . When the system subjects to dephasing environment, however, both $f(t_0)$ and $F(t_0)$ decrease with the increase of N and r . Moreover, the critical decoherence rate γ_c

before which the decoherence spin channel is superior to its classical counterpart is independent of N for dissipative environment, and it decreases with the increase of N for dephasing environment.

For entanglement distribution and creation, our results revealed that the distributed entanglement shows completely the same dynamical behaviors when the system subjects to dissipative or dephasing environment, and for fixed γ , the maximum value of the concurrence $C_{\text{NI,B}}$ decreases as N increases, and when $N \rightarrow \infty$, $C_{\text{NI,B}}(t_c) = e^{-\gamma\pi/2\lambda}$. The created entanglement also decreases as N increases, and for the case of dissipative environment, the maximum concurrence C approaches its asymptotic value $C(t_c) = 2e^{-(\gamma\pi/2\lambda)}/N_A$ in the limit of $N \rightarrow \infty$, while for the case of dephasing environment, its asymptotic value can only be obtained numerically.

From the above analysis it can be seen that both the dissipative and dephasing environments have severe detrimental effects on transport capacity of a spin channel, thus a question naturally arises at this stage is how to stabilize a quantum system against this unwanted phenomenon, or in other words, how to minimize, delay or even eliminate the detrimental effects of decoherence. In a recent work [51], we have shown that for some specific environments, it is possible to obtain a near perfect state transfer by adjusting the coupling strengths between neighboring qubits of a spin network, however, for decoherence modes considered here, this procedure cannot be applied, thus one must resort to other techniques in order to get a high efficient communication. Physically, one can increase the transfer fidelity to some degree by increasing the coupling strength between neighboring qubits of the spin network, or equivalently, by increasing the scaling constant λ (this statement can be proved true by the explicit form of the operator \tilde{A} , from which one can obtain that increasing λ will decrease the period of the suppressed oscillation and thus enlarges the maximum value of the state transfer fidelity). Particularly, in the limit of $\lambda \rightarrow \infty$, the transfer fidelity will approaches unity. However, the realization of λ large enough to obtain high efficient communication might be a difficult experimental task.

Finally, we would like to emphasize that although there are works showing that efficiency of the quantum state transfer can sometimes be enhanced to some extent by decoherence [52, 53, 54], finding ways to minimize or even eliminate the detrimental effects of decoherence is still the prerequisites and challenging task in the practical realization of quantum computer.

This work was supported by the Natural Science Foundation of Shaanxi Province under Grant Nos. 2009JQ8006 and 2009GM1007, the Specialized Research Program of Education Bureau of Shaanxi Province under Grant No. 08JK434, and the Youth Foundation of Xi'an University of Posts and Telecommunications under Grant No. ZL2008-11.

References

1. S. Bose, Phys. Rev. Lett. **91**, 207901 (2003)
2. T.J. Osborne, N. Linden, Phys. Rev. A **69**, 052315 (2004)
3. M. Christandl, N. Datta, A. Ekert, A.J. Landahl, Phys. Rev. Lett. **92**, 187902 (2004)
4. M. Christandl, N. Datta, T.C. Dorlas, A. Ekert, A. Kay, A.J. Landahl, Phys. Rev. A **71**, 032312 (2005)
5. Y. Li, T. Shi, B. Chen, Z. Song, C.P. Sun, Phys. Rev. A **71**, 022301 (2005)
6. T. Shi, Y. Li, Z. Song, C.P. Sun, Phys. Rev. A **71**, 032309 (2005)
7. M.-H. Yung, S. Bose, Phys. Rev. A **71**, 032310 (2005)
8. D. Burgarth, S. Bose, Phys. Rev. A **71**, 052315 (2005)
9. D. Burgarth, S. Bose, New J. Phys. **7**, 135 (2005)
10. I. D'Amico, B.W. Lovett, T.P. Spiller, Phys. Rev. A **76**, 030302 (2007)
11. A. Wójcik, T. Łuczak, P. Kurzyński, A. Grudka, T. Gdala, M. Bednarska, Phys. Rev. A **72**, 034303 (2005)
12. R.H. Crooks, D.V. Khveshchenko, Phys. Rev. A **77**, 062305 (2008)
13. J.F. Zhang, G.L. Long, W. Zhang, Z.W. Deng, W.Z. Liu, Z.H. Lu, Phys. Rev. A **72**, 012331 (2005)
14. V. Kostak, G.M. Nikolopoulos, I. Jex, Phys. Rev. A **75**, 042319 (2007)
15. M.A. Jafarizadeh, R. Sufiani, Phys. Rev. A **77**, 022315 (2008)
16. G. Gualdi, V. Kostak, I. Marzoli, P. Tombesi, Phys. Rev. A **78**, 022325 (2008)
17. M. Paternostro, G.M. Palma, M.S. Kim, G. Falci, Phys. Rev. A **71**, 042311 (2005)
18. A. Kay, Phys. Rev. A **73**, 032306 (2006)
19. J.F. Zhang, X.H. Peng, D. Suter, Phys. Rev. A **73**, 062325 (2006)
20. O. Romero-Isart, K. Eckert, A. Sanpera, Phys. Rev. A **75**, 050303 (2007)
21. C. Di Franco, M. Paternostro, M.S. Kim, Phys. Rev. Lett. **101**, 230502 (2008)
22. C. Di Franco, M. Paternostro, D.I. Tsomokos, S.F. Huelga, Phys. Rev. A **77**, 062337 (2008)
23. M. Markiewicz, M. Wieśniak, Phys. Rev. A **79**, 054304 (2009)
24. X.X. Yi, H.T. Cui, X.G. Wang, Phys. Lett. A **306**, 285 (2003)
25. A.R.R. Carvalho, F. Mintert, A. Buchleitner, Phys. Rev. Lett. **93**, 230501 (2004)
26. J. Wang, H. Batelaan, J. Podany, A.F. Starace, J. Phys. B **39**, 4343 (2006)
27. A. Abliz, H.J. Gao, X.C. Xie, Y.S. Wu, W.M. Liu, Phys. Rev. A **74**, 052105 (2006)
28. M.L. Hu, X.Q. Xi, C.X. Li, H.Z. Qu, Physica B **404**, 16 (2009)
29. M.L. Hu, X.Q. Xi, H.L. Lian, Physica B **404**, 3499 (2009)
30. M. Hein, W. Dür, H.-J. Briegel, Phys. Rev. A **71**, 032350 (2005)
31. J.M. Cai, Z.W. Zhou, G.C. Guo, Phys. Rev. A **74**, 022328 (2006)
32. Z. Sun, X.G. Wang, Y.B. Gao, C.P. Sun, Eur. Phys. J. D **46**, 521 (2008)
33. A. Montakhab, A. Asadian, Phys. Rev. A **77**, 062322 (2008)
34. Z.G. Li, S.M. Fei, Z.D. Wang, W.M. Liu, Phys. Rev. A **79**, 024303 (2009)

35. L. Zhao, H. Fan, Phys. Rev. A **79**, 064305 (2009)
36. A.R.P. Rau, M. Ali, G. Alber, Eur. Phys. Lett. **82**, 40002 (2008)
37. M. Ali, G. Alber, A.R.P. Rau, J. Phys. B **42**, 025501 (2009)
38. F. Mintert, A.R.R. Carvalho, M. Kuś, A. Buchleitner, Phys. Rep. **415**, 207 (2005)
39. Lindblad, Commun. Math. Phys. **48**, 199 (1976)
40. L.M. Arévalo-Aguilar, H. Moya-Cessa, Quantum Semi-class. Opt. **10**, 671 (1998)
41. H.X. Lu, J. Yang, Y.D. Zhang, Z.B. Chen, Phys. Rev. A **67**, 024101 (2003)
42. D.F. Walls, G.J. Milburn, *Quantum Optics*, 2nd edn. (Springer, Berlin, 2007)
43. M.D. Bowdrey, D.K.L. Oi, A.J. Short, K. Banaszek, J.A. Jones, Phys. Lett. A **294**, 258 (2002)
44. D. Loss, D.P. DiVincenzo, Phys. Rev. A **57**, 120 (1998)
45. M.L. Hu, X.Q. Xi, Acta Phys. Sin. **57**, 3319 (2008)
46. M. Horodecki, P. Horodecki, R. Horodecki, Phys. Rev. A **60**, 1888 (1999)
47. W.K. Wootters, Phys. Rev. Lett. **80**, 2245 (1998)
48. T. Yu, J.H. Eberly, Opt. Commun. **264**, 393 (2006)
49. Á. Perales, M.B. Plenio, J. Opt. B **7**, S601 (2005)
50. W. Dür, G. Vidal, J.I. Cirack, Phys. Rev. A **62**, 062314 (2000)
51. M.L. Hu, L.H. Lian, Eur. Phys. J. D **55**, 711 (2009)
52. M.P. Plenio, S.F. Huegla, New J. Phys. **10**, 113019 (2008)
53. P. Rebentrost, M. Mohseni, I. Kassal, S. Lloyd, A. Aspuru-Guzik, New J. Phys. **11**, 033003 (2009)
54. F. Caruso, A.W. Chin, A. Datta, S.F. Huegla, M. P. Plenio, J. Chem. Phys. **131**, 105106 (2009)